Investigation of Metal Ion Uptake Reactivities of [3Fe-4S] Clusters in Proteins: Voltammetry of Co-Adsorbed Ferredoxin-Aminocyclitol Films at Graphite Electrodes and Spectroscopic Identification of Transformed Clusters

Julea N. Butt,[†] Fraser A. Armstrong,*[,†] Jacques Breton,[‡] Simon J. George,[‡] Andrew J. Thomson,[‡] and E. Claude Hatchikian[§]

Contribution from the Department of Chemistry, University of California, Irvine, California 92717. School of Chemical Sciences, University of East Anglia, Norwich, NR4 7TJ U.K., and Laboratoire de Chimie Bacterienne, CNRS, PB 71, 13277, Marseille, France. *Received March 5, 1991*

Abstract: Facile transformation of Fe-S clusters in proteins, as described by $[3Fe\text{-}4S]^0 + M^{2+} \rightleftharpoons [M3Fe\text{-}4S]^{2+}$ in which metal ion M enters the vacant subsite of a 3Fe cluster to complete a cubane-type structure, is identified and studied by a convenient and highly economical voltammetric procedure. The technique extends a recent discovery that ferredoxins coadsorb with aminocyclitols at a pyrolytic graphite "edge" (PGE) electrode, giving a stable electroactive film, and is demonstrated by an investigation of cluster interconversions in *Desulfovibrio africanus* ferredoxin III (Fd III). Cyclic voltammetric scanning (typically over the region 0 to -850 mV vs SHE) of a preformed film, transferred to an EGTA-containing buffer solution at pH 7, reveals well-defined voltammetric signals due to three redox couples. One of these (B′) corresponds to the stable $[4Fe\text{-}4S]^{2+/+}$ cluster; the other two (A′ and C′) are associated with the [3Fe-4S] cluster and assigned respectively as the normal 1+/0 couple and a chemically reversible two-electron process of as yet unestablished formulation. If the coated electrode is then transferred to stirred solutions devoid of EGTA but containing low concentrations of Fe^{2+}, Zn^{2+}, or Cd^{2+}, reductive passage through couple A′ ($[3Fe\text{-}4S]^{+/0}$) initiates rapid changes. During subsequent cycles over the course of several seconds, waves A′ and C′ disappear simultaneously and are replaced by a new couple $D'_{(M)}$. Values of $E^{o'}$ are as follows: $D'_{(Fe)}$, -393 ± 10 mV; $D'_{(Zn)}$, -492 ± 10 mV; $D'_{(Cd)}$, -569 ± 10 mV. The positions of the new couples correspond closely with cyclic voltammograms of Fd III undergoing transformations in the solution phase. Characterization by EPR and MCD spectroscopy identifies the latter species to be $[4Fe\text{-}4S]^{2+/+}$, $[Zn3Fe\text{-}4S]^{2+/+}$, and $[Cd3Fe\text{-}4S]^{2+/+}$, respectively. The clusters $[Zn3Fe\text{-}4S]^{2+}$ and $[Cd3Fe\text{-}4S]^{2+}$ are shown to be isoelectronic with $[3Fe\text{-}4S]^0$ and to have a ground electronic state $S = 2$ subject to a negative axial zero-field splitting. The reduced states $[Zn3Fe\text{-}4S]^+$ and $[Cd3Fe\text{-}4S]^+$ have a ground state spin $S = {}^5/_2$ with characteristic EPR spectra. Rates and equilibria of metal ion uptake for protein molecules confined to the electrode surface depend upon the identity and concentration of the metal ion. Values of K_d, the equilibrium dissociation constant given by $\{[M^{2+}]\{[3Fe\text{-}4S]^0\}/\{[M3Fe\text{-}4S]^{2+}\}$ are as follows: Fe, 30 ± 15 μM; Zn, 1.6 ± 1.0 μM; Cd, 0.8 ± 0.5 μM. The affinity order $Cd^{2+} \geq Zn^{2+} \gg Fe^{2+}$ is thus established. The results demonstrate the feasibility of an intrinsic preference for Zn (a biologically abundant element) as compared to Fe, at the M subsite of [M3Fe-4S] clusters in proteins.

Introduction

It is now widely accepted that iron-sulfur clusters in certain proteins undergo facile, reversible transformations described by (1) in which metal ion M enters the vacant subsite of a 3Fe cluster to complete a cubane-type structure. Such reactions account for

$$[3Fe\text{-}4S]^0 + M^{2+} \rightleftharpoons [M3Fe\text{-}4S]^{2+} \qquad (1)$$

the activation of inactive aconitase in which the incorporated Fe is coordinatively differentiated and catalytically active.[1,2] Cluster interconversions have been identified in other proteins, particularly ferredoxin III (Fd III) from *Desulfovibrio africanus*,[3] the ferredoxin from *Desulfovibrio gigas* for which several cubane-type products (M = Fe, Co, Zn) have been characterized by EPR and Mössbauer,[4-6] and the ferredoxin from *Pyrococcus furiosus*[7] for which formation of a [Ni3Fe-4S] cluster has also been reported.[8] One approach toward understanding the underlying chemistry is through the synthesis and detailed characterization of pertinent analogues, for example subsite-differentiated cubane structures based upon the Fe_3S_4 core.[9] However, several factors make it difficult to identify and clarify such reactivity in proteins themselves. These include the broad, rather featureless UV-visible spectra of most Fe-S clusters and the consequential need to use low-temperature EPR, MCD, or Mössbauer spectroscopy to determine if reaction has occurred; the substantial sample requirements of these techniques (which for proteins in scarce supply may be prohibitive); and the difficulty of reversibly manipulating unstable proteins and metal ions under critical conditions of controlled low potential. In addition, it would be highly desirable to have the ability to quantify dynamic equilibria at the tight-binding level (dissociation constants of micromolar or lower). We have now discovered that specific cluster transformations in ferredoxins can be identified and investigated by a rapid voltammetric procedure that uses, in practice, a fraction of a nanomole per experiment and permits equilibrium and kinetic parameters to be obtained. The technique extends our recent discovery[10] that ferredoxins coadsorb with aminocyclitols at a pyrolytic graphite "edge" (PGE) electrode giving a stable electroactive film. We demonstrate its utility here by conducting and visualizing cluster interconversions in Fd III from *D. africanus*.

The amino acid sequence of Fd III (MW 6600)[11] shows the presence of seven cysteine residues. Four of them bind one

[†] University of California.
[‡] University of East Anglia.
[§] CNRS.

(1) Beinert, H.; Kennedy, M. C. *Eur. J. Biochem.* **1989**, *186*, 5.
(2) Robbins, A. H.; Stout, C. D. *Proc. Natl. Acad. Sci. U.S.A.* **1989**, *86*, 3639.
(3) George, S. J.; Armstrong, F. A.; Hatchikian, E. C.; Thomson, A. J. *Biochem. J.* **1989**, *264*, 275.
(4) Moura, J. J. G.; Moura, I.; Kent, T. A.; Lipscomb, J. D.; Huynh, B.-H.; LeGall, J.; Xavier, A. V.; Münck, E. *J. Biol. Chem.* **1982**, *257*, 6259.
(5) Moura, I.; Moura, J. J. G.; Münck, E.; Papaefthymiou, V.; LeGall, J. *J. Am. Chem. Soc.* **1986**, *108*, 349.
(6) Surerus, K. K.; Münck, E.; Moura, I.; Moura, J. J. G.; LeGall, J. *J. Am. Chem. Soc.* **1987**, *109*, 3805.
(7) Conover, R. C.; Kowal, A. T.; Fu, W.; Park, J.-B.; Aono, S.; Adams, M. W. W.; Johnson, M. K. *J. Biol. Chem.* **1990**, *265*, 8533.
(8) Conover, R. C.; Park, J.-B.; Adams, M. W. W.; Johnson, M. K. *J. Am. Chem. Soc.* **1990**, *112*, 4562.
(9) Ciurli, S.; Carrie, M.; Weigel, J. A.; Carney, M. J.; Stack, T. D. P.; Papaefthymiou, G. C.; Holm, R. H. *J. Am. Chem. Soc.* **1990**, *112*, 2654.
(10) Armstrong, F. A.; Butt, J. N.; George, S. J.; Hatchikian, E. C.; Thomson, A. J. *FEBS Lett.* **1989**, *259*, 15.
(11) Bovier-Lapierre, G.; Bruschi, M.; Bonicel, J.; Hatchikian, E. C. *Biochim. Biophys. Acta* **1987**, *913*, 20.

0002-7863/91/1513-6663$02.50/0

[4Fe-4S] cluster, and three are available to ligate the [3Fe-4S] center.[12] Between the cysteine residues at positions 11 and 17 lies an aspartate group, position 14, instead of cysteine as would be found in a typical 2[4Fe-4S] ferredoxin.[13] The $[3Fe\text{-}4S]^0$ cluster incorporates Fe^{2+} rapidly to form a [4Fe-4S] cluster that has novel magnetic properties.[3] It is most likely that the entering Fe occupies the subsite adjacent to Asp. In this study we have used the film voltammetry technique to compare the reactions of $[3Fe\text{-}4S]^0$ with various metal ions—Fe^{2+}, Zn^{2+}, and Cd^{2+}—under strict potential control. As a biological trace metal, Zn has an abundance similar to that of Fe.[14]

Experimental Section

Ferredoxin III from *D. africanus* strain Benghazi (NCIB 8401) was isolated as described previously[15] and stored as frozen pellets in liquid N_2. Samples used in experiments had a purity index (A_{408}/A_{280}) of 0.78. For subsequent operations all solutions were made from purified water of resistivity ~18 MΩ·cm (Barnstead Nanopure). Ferredoxin solutions were prepared for studies by diafiltration against buffer solutions at 4 °C on an Amicon 8MC unit equipped with a microvolume assembly and a YM5 membrane. Final concentrations were determined from the absorption coefficient 28.6 mM^{-1} cm^{-1} at 408 nm. For voltammetry of films, the buffer electrolyte was 0.10 M NaCl (Aldrich or BDH Aristar) containing 20 mM Hepes or a mixed-buffer component made of 5 mM each in acetate (from acetic acid; Aldrich) and Mes, Hepes, and Taps (Sigma) adjusted to pH 7.0 at 4 °C. Neomycin sulfate (Sigma) was added as a 0.2 M stock solution adjusted to pH 7.2. Small aliquots of EGTA (ethene glycol-*O,O'*-bis(2-aminoethyl)-*N,N,N',N'*-tetraacetic acid; Aldrich; adjusted to pH 7.0; used to sequester free Fe^{2+}), HPDTA (2-hydroxy-1,3-diaminopropane-*N,N,N',N'*-tetraacetic acid; Aldrich; adjusted to pH 7.0; used to sequester free Fe^{2+} in the presence of Cd^{2+}), Fe^{2+} ($(NH_4)_2Fe(SO_4)_2 \cdot 6H_2O$; Aldrich), Zn^{2+} ($ZnSO_4 \cdot 7H_2O$; Aldrich), or Cd^{2+} ($CdCl_2 \cdot 2.5H_2O$; Aldrich) were each added as required from concentrated Ar-purged stock solutions. Solutions of sodium dithionite (BDH) were prepared and kept in a glovebox.

Cyclic voltammetric experiments were carried out with use of an all-glass cell that was a modification of the type described in an earlier report.[12] It comprised a centrally located reference compartment, equipped with a circulating jacket, linked radially by Luggin capillary arms to four small-volume sample pots. The standard calomel reference electrode (SCE) was positioned in the central compartment and maintained at 25 °C (at which E_{SCE} is 244 mV vs the standard hydrogen electrode (SHE)). The sample pots, each holding 500–600 μL of electrolyte solution containing either EGTA or the particular metal ion under investigation, were immersed in a cooling bath maintained at 0 °C. These solutions were deoxygenated by passing humidified O_2-free argon across the surface while stirring by magnetic microflea. The auxiliary electrode in each sample pot was a piece of Pt gauze positioned opposite to the Luggin tip. The pyrolytic graphite edge (PGE) electrode was constructed as described previously.[12] For each experiment this was polished with an aqueous alumina slurry (Buehler Micropolish, 0.3 or 1.0 μm) and sonicated extensively to remove traces of Al_2O_3. At all times during voltammetry, the PGE surface was positioned close to the Luggin tip.

For preparation of heteroatom clusters in solution, stock solutions of Fd III were dialyzed (using the ultrafiltration cell) against an aerobic solution of Hepes (0.20 M, pH 7.6) containing EGTA equimolar with protein. This procedure removed contaminating Fe. Following further dialysis into Hepes or Taps buffers containing 0.1 M KCl and either EGTA or HDPTA, samples were transferred to an anaerobic glovebox. Two procedures were used for carrying out cluster transformations. For preparation of concentrated samples for optimal-quality MCD and EPR spectroscopy, mediated chemical titration was the method of choice in most cases. A standard cell of the type described by Dutton with Pt wire and SCE electrodes was used.[16] For MCD, the glassing agent ethane-1,2-diol (ED) was added to 50% (v/v) dilution. The following dyes were added (final concentrations typically 20 μM in each) to establish redox equilibrium at various potentials during titrations with sodium dithionite ($E^{0'}$ values given vs SHE[17]): indigo carmine, −135 mV; anthraquinone-2,6-disulfonate, −205 mV; phenosafranine, −280 mV; benzylviologen, −345 mV; methylviologen, −445 mV. Sodium dithionite was titrated into the cell until the observed potential came into the region of approximately −300 mV, within which the [3Fe-4S] cluster is reduced while the [4Fe-4S] cluster remains oxidized.[12] (Preparation of the sample of $[3Fe\text{-}4S]^0$ used for MCD was carried out by addition of reduced phenosafranine.) Aliquots of Zn^{2+} or Cd^{2+} stock solutions were then added to give a 4-fold excess over the protein concentration. Protein concentrations were in the region 200–400 μM. Such a procedure produced heteroatom clusters in the oxidation level $[M3Fe\text{-}4S]^{2+}$. To obtain the *reduced* Zn heteroatom cluster $[Zn3Fe\text{-}4S]^+$, the potential was then lowered further by dithionite additions to a final potential of −535 mV. From the reduction potentials determined (vide infra) this potential was sufficient to reduce 90% of the Zn cluster population, but in analogous experiments with Cd^{2+} it was not sufficiently negative to produce significant amounts of $[Cd3Fe\text{-}4S]^+$. To prepare the latter species and, more generally, to enable bulk solution cyclic voltammetry to be undertaken on all transformed samples, direct bulk electrolysis was employed. This was carried out with a three-chamber cell assembly that was used inside an anaerobic glovebox. The cell was broadly similar to that described previously[12] except that the working electrode consisted of a cylindrical block of PGE (1.2-cm length and 0.9-cm diameter, the ends being basal plane surface) through which was bored a concentric hole of 0.6-cm diameter. The inside walls thus projected the "edge" surface. The sample pot was completed by a base of PGE cemented to the lower end with insulating epoxy (this was wired separately so that cyclic voltammetry, at a planar surface, could be conducted at intervals during the course of electrolysis) and a thin glass outer wall allowing it to be inserted into a thermostated jacket. The resulting high surface area PGE cell gave reduction half-times of the order of 10 min for a solution 400 μL in volume. In each case, electrochemistry was promoted by addition of neomycin to a final concentration of 2 mM. Typical ferredoxin concentrations for electrolysis were in the region of 100 μM. Higher protein concentrations resulted in poor electrochemistry and slow reduction.

Cyclic voltammetry and bulk electrolysis were carried out with use of an Ursar Instruments potentiostat for which calibration and performance were checked regularly over the period of studies. Voltammograms were recorded with a Kipp and Zonen XY recorder. Formal reduction potentials $E^{0'}$ were determined from the average of reduction (cathodic) and oxidation (anodic) peak potentials $(E_{pc} + E_{pa})/2$.

EPR spectra were recorded at Norwich on a Bruker ER-200D X-band spectrometer equipped with a helium flow cryostat (ESR-9, Oxford Instruments, plc). Low-temperature MCD measurements were made on a Jasco J-500D dichrograph and split-coil superconducting magnet SM-4. Procedures for measuring EPR and MCD spectra have been described previously.[12] UV–visible absorption spectra were recorded with a Hitachi 3200 spectrometer.

Results and Discussion

To prepare films, about 2 μL of an ice-cold solution of Fd III, typically 100 μM in 0.1 M NaCl, mixed buffer (5 mM each in acetate, Hepes, Mes, and Taps, pH 7) containing 2 mM neomycin sulfate, and 100 μM EGTA were spread evenly across the surface (area ca. 0.2 cm^2) of a freshly polished, chilled PGE electrode. When transferred promptly into an electrolyte solution also containing 2 mM neomycin, and with 10 μM EGTA, cyclic voltammetric scanning over the region 0 to ca. −850 mV (vs SHE) reveals three redox couples. After several cycles at 0 °C the signals become established at a constant amplitude (see ref 19) and provided the lower switching potential is not permanently maintained more negative than −850 mV, they show only a small rate of further attenuation (typically 20% over 20 min). No signals are obtained if neomycin is absent from coating and cell solutions, while an unstable rapidly diminishing response is observed if an electrode coated as described above is transferred to a cell devoid of neomycin. These observations show that neomycin is essential for obtaining an electroactive layer of adsorbed protein molecules and suggest that it stabilizes such a layer by dynamically independent coadsorption. The voltammogram observed after several cycles is shown in Figure 1.

(12) Armstrong, F. A.; George, S. J.; Cammack, R.; Hatchikian, E. C.; Thomson, A. J. *Biochem. J.* **1989**, *264*, 265.

(13) Fukuyama, K.; Nagahara, Y.; Tsukihara, T.; Katsube, Y.; Hase, T.; Matsubara, H. *J. Mol. Biol.* **1988**, *199*, 483: Otaka, E.; Ooi, T. *J. Mol. Evol.* **1987**, *27*, 257.

(14) Williams, R. J. P. In *Zinc in Human Biology*; Mills, C. F., Ed.; Springer-Verlag: Berlin, Heidelberg, 1989; Chapter 2. See also other chapters in this book.

(15) Hatchikian, E. C.; Bruschi, M. *Biochim. Biophys. Acta* **1981**, *634*, 41.

(16) Dutton, P. L. *Methods in Enzymology*; Academic Press: New York, 1978; Vol. 54, pp 411–435.

(17) Wilson, G. S. *Methods in Enzymology*; Academic Press: New York, 1978; Vol. 54, pp 396–410. Prince, R. C.; Linkletter, S. J. G.; Dutton, P. L. *Biochim. Biophys. Acta* **1981**, *635*, 132.

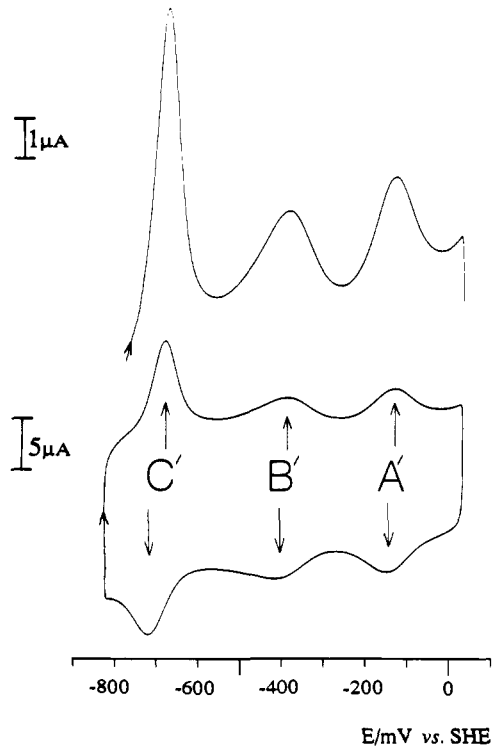

Figure 1. Steady-state cyclic voltammogram of a film of 7Fe ferredoxin III. Upper trace is an oxidative sweep measured at higher gain. The film was prepared from a 100 μM solution of ferredoxin in buffer–electrolyte (see text). Scanning was performed in buffer electrolyte, pH 7, containing 2 mM neomycin and 10 μM EGTA. Temperature 0 °C. The voltammograms, measured at a scan rate of 190 mV s^{-1}, follow a few excursions into the potential region below −950 mV. This has sharpened waves B′.

Wave pairs A′, B′, and C′[18] (corresponding to waves A, B, and C observed when Fd III is present in solution[12]) have been assigned[10] respectively to the couples $[3Fe\text{-}4S]^{+/0}$, $[4Fe\text{-}4S]^{2+/+}$, and (tentatively) $[3Fe\text{-}4S]^{0/2-}$. Attainment of a 2− oxidation level (formally all Fe(II)) has yet to be confirmed spectroscopically. All waves in the steady-state voltammogram are well-defined, those for couple A′ exhibiting the most straightforward behavior.[19] At a scan rate of 190 mV s^{-1}, waves A′ have a half-height width of ca. 100 mV that may be compared with the theoretical value 85 mV (0 °C) expected[20] for ideal Langmuir behavior (that is, for rapid one-electron exchange with a homogeneous population of mutually noninteracting adsorbed species). Peak to peak separations ($E_{pa}-E_{pc}$) for A′ are less than 50 mV even at a scan rate of 470 mV s^{-1}, thus indicating that electron transfer is fast.[21]

Rapid and dramatic changes are observed if the coated electrode is then transferred (wet) into stirred solutions devoid of EGTA but containing low concentrations of Fe^{2+}, Zn^{2+}, or Cd^{2+}. In each case, following a brief holding period at approximately 0 mV (during which the solution is stirred to disperse trace amounts of EGTA carried over) reductive passage through wave A′ initiates a rapid reaction. As illustrated in Figure 2, the course of this reaction is clearly evident from successive cycles over the range 0 to −800 mV. For clarity, only the oxidation waves are shown, each scan offset vertically. Waves A′ and C′ disappear to be replaced by a pair due to a new couple $D'_{(M)}$. By taking pairs of reference points at appropriate potentials across the voltammogram and plotting the differential current amplitudes as a function of time in semilogarithmic form, it was determined that these changes occur in a concerted manner and conform to first-order kinetics. In each case, plots were linear for at least 70% reaction and time constants for disappearance of A′ and C′ matched those for appearance of D′. The reversibility of each reaction (i.e., D′ → A′ + C′) could be confirmed by performing a further, subsequent operation with the transformed protein. In each case, transfer of the electrode *back* to a pot containing a solution of EGTA instead of M^{2+} produced voltammograms identical with that of Figure 1 after several cycles over the same potential range.

We made no attempt here to interpret rates of change in an absolute sense, since these will depend upon the species being "redox-switched" during the cycle and must therefore be a complex function of the range and rate of the scan. However, restricting our analysis to relative terms, it was clear that rates (and equilibrium extents) of the reactions did depend upon the identity of the metal ion and its concentration. Importantly, the affinity order $Cd^{2+} \sim Zn^{2+} > Fe^{2+}$ was reproducibly observed for each of numerous experiments (see later text). At this stage, wishing to emphasize the immediate, visual aspects of this work, we have (for Figure 2) chosen respective concentrations for each metal ion that give similar rates and result in >90% reaction. Voltammograms of the final states are shown in Figure 3 (left). For the new couples $D'_{(M)}$, values of $E^{0'}$ are as follows: $D'_{(Fe)}$, −393 ± 10 mV (appearing as an intensification of wave B′); $D'_{(Zn)}$, −492 ± 10 mV; $D'_{(Cd)}$, −569 ± 10 mV. Where the local base line could be estimated easily, the increase in integrated area due to D′ was found to be equal (within 10%) to the original area under A′. Such an analysis was possible, for example, in the case of complete reaction with Cd^{2+} for which D′ is quite well separated from the somewhat broader wave B′ and there is no contribution from C′. In the case of reaction with Fe^{2+}, the combined area defined by waves B′ and D′ of the product was within 10% of that defined by the original waves A′ and B′. Thus, waves D′ are due to a one-electron couple that replaces A′ (one electron) and C′ (two electrons). In each case, waves D′ appear well-defined with half-height widths of about 100 mV indicating that the degree of "ideality" (species homogeneity and absence of interaction between redox sites) is very similar to that of the original waves A′. Furthermore, peak separations ($E_{pa} - E_{pc}$) for couple D′ were in each case less than 50 mV at 470 mV s^{-1}, again as observed for A′.

To determine that these surface-executed reactions were a true reflection of processes occurring in bulk solution (albeit requiring orders of magnitude more sample for examination), we carried out several experiments designed to characterize the corresponding products of bulk solution chemistry. The first such test was the appearance of cyclic voltammograms (Figure 3, right) obtained with solutions of Fd III, in each case after two-electron bulk reduction of the 7Fe protein followed by titration with Fe^{2+}, Zn^{2+}, or Cd^{2+} (vide infra). The $E^{0'}$ values for the new couples ($D_{(Fe)}$, −400 ± 15 mV;[3] $D_{(Zn)}$, −480 + 15 mV; $D_{(Cd)}$, −580 + 10 mV) are

(18) We have adopted the use of superscript prime to refer to the redox couples observed for protein molecules adsorbed at the surface as opposed to those for the free protein in solution.

(19) We have noted that the positions of all waves shift during the first few cycles over the range between +100 and −850 mV. Waves due to couples A′ and C′ each shift by approximately +15 mV, but a larger, potential-dependent change is observed for waves B′. Waves B′ are influenced significantly by the applied electrode potential: Initially, the signals are spread over about 300 mV with the peak positions located at around −480 mV; however, following two or three cycles with the cathodic switching potential temporarily lowered to −950 mV, they sharpen up to give a half-height width of ca. 120 mV with the average peak potential located at −390 mV. This can be seen in Figure 1. Prolonged periods of cycling once again over the range +100 to −850 mV causes waves B′ to revert back to the broadened form (this is clearly apparent in the voltammograms of the transformed proteins that are shown in Figures 2 and 3). Such shifts may reflect a potential-dependent adjustment of the microenvironment or orientation of adsorbed proteins, to which the [4Fe-4S] cluster is clearly much more sensitive than [3Fe-4S]. The appearance of couple C′ is sensitive to pH and scan rate. Effects are particularly pronounced for the reduction wave: As either pH or scan rate is increased, this wave broadens and takes on a "tail" indicating chemical complications in the reduction process (see ref 10). On the basis of the integrated current response for couple A′, the coverage can be estimated to be in the order of approximately one effective monolayer based upon a geometric surface area of 0.20 cm^2 and allowing each protein molecule to occupy an area of 500 $Å^2$. A similar conclusion could be drawn on the basis of the integrated current responses for B′ or the oxidation wave of couple C′ (two electrons).

(20) Laviron, E. *Bull. Soc. Chim. Fr.* **1970**, 1637; *J. Electroanal. Chem. Interfacial Electrochem.* **1974**, *52*, 355, 395.

(21) Laviron, E. *J. Electroanal. Chem. Interfacial Electrochem.* **1979**, *101*, 19.

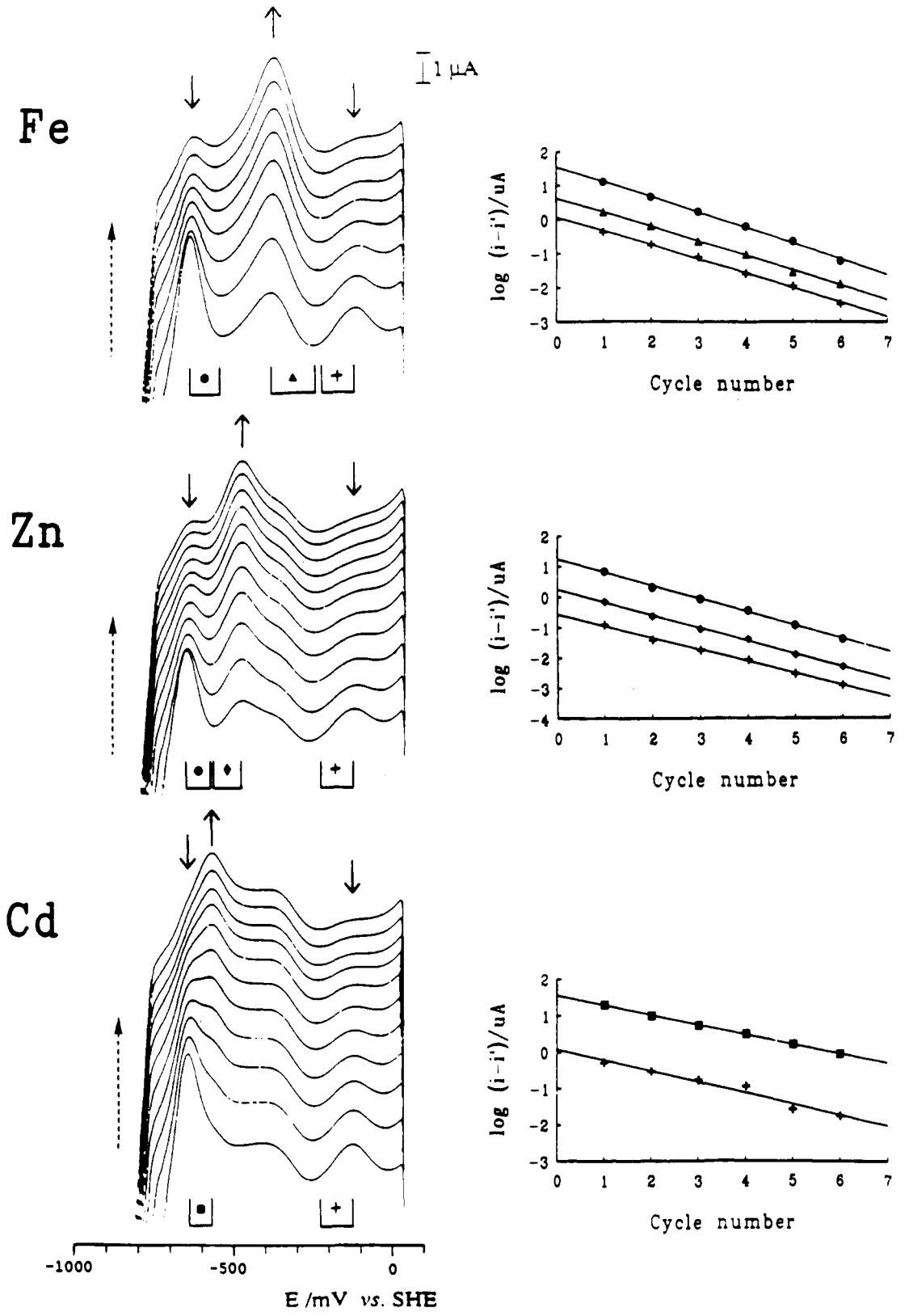

Figure 2. Left: Oxidative scans (successive cycles) of a film of 7Fe ferredoxin III upon transfer to M^{2+} solutions. Right: Corresponding semilog plots showing time correspondence of appearance of waves D′ and disappearance of waves A′ and C′. Initial films of 7Fe ferredoxin were prepared as described in the text and as employed for Figure 1. The potential was held briefly at ca. +50 mV prior to commencement of scanning at 470 mV s^{-1}. Temperature 0 °C. Each determination involved measurement of the difference in current at two potentials as indicated. These are as follows. Fe^{2+} (300 μM): +, $i_{-129mV} - i_{-229mV}$, couple A′; ▲, $i_{-393mV} - i_{-250mV}$, couple D′; ●, $i_{-651mV} - i_{-554mV}$, couple C′. Zn^{2+} (10 μM): +, $i_{-129mV} - i_{-229mV}$, couple A′; ▲, $i_{-484mV} - i_{-570mV}$, couple D′; ●, $i_{-655mV} - i_{-579mV}$, couple C′. Cd^{2+} (10 μM): +, $i_{-129mV} - i_{-229mV}$, couple A′; ■, $i_{-641mV} - i_{-568mV}$, combination of couples C′ and D′.

close to those observed for the adsorbed films. In view of our previous characterization of the M = Fe product and its assignment as a [4Fe-4S] cluster,[3] the underlying similarity in behavior now observed for M = Zn or Cd and the marked sensitivity of the product reduction potential to the identity of M together indicated that Zn^{2+} or Cd^{2+} add to the one-electron-reduced

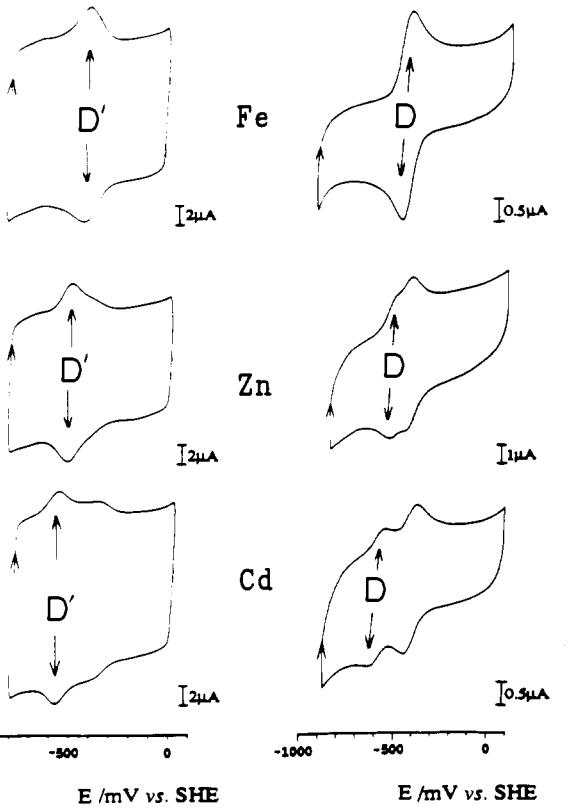

Figure 3. Left: Final voltammograms of films of transformed ferredoxin III scanned in buffer electrolyte, showing positions of couple D′: Fe, 650 μM; Zn, 15 μM; Cd, 10 μM. Scan rate 470 mV s^{-1}; temperature 0 °C. All other conditions as described in the text. Note that buffer electrolyte contains no EGTA. Right: Final voltammograms of bulk solutions of transformed ferredoxin III, showing positions of couple D. Key: Fe, 105 μM; ferredoxin III, 105 μM; buffer electrolyte at pH 7.4 containing 1.5 mM neomycin; temperature 4 °C; scan rate 10 mV s^{-1}. Zn, 200 μM; ferredoxin, 100 μM; EGTA, 100 μM; buffer electrolyte at pH 7.1 containing 2 mM neomycin; temperature 3 °C; scan rate 19 mV s^{-1}. Cd, 200 μM; ferredoxin, 100 μM; EGTA, 100 μM; buffer electrolyte at pH 7.4 containing 2 mM neomycin; temperature 3 °C; scan rate 5 mV s^{-1}.

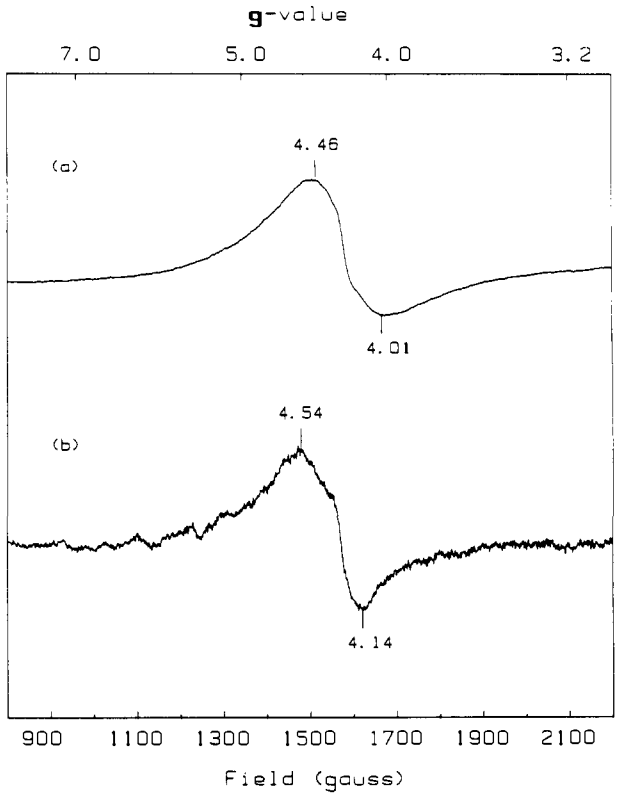

Figure 4. X-band EPR spectra of $[M3Fe\text{-}4S]^+$. (a) $[Zn3Fe\text{-}4S]^+$: Fd III, 300 μM; $ZnSO_4$, 660 μM; 0.5 M Taps buffer, pH 8.2, 0.1 M KCl, including 20 μM mediator dyes (see text). Sample was titrated with $Na_2S_2O_4$ to a potential of −535 mV vs SHE. Conditions: microwave power 20 mW; frequency 9.38 GHz; modulation amplitude 1.0 mT; sample temperature 14.0 K. (b) $[Cd3Fe\text{-}4S]^+$: Fd III, 100 μM; $CdCl_2$, 330 μM; 0.2 M Hepes buffer, pH 7.3, 0.1 M KCl, containing 225 μM HPDTA. Sample was electrochemically reduced at −650 mV vs SHE. Conditions: microwave power 32 mW; frequency 9.38 GHz; modulation amplitude 1.0 mT; sample temperature 7.0 K.

[3Fe-4S] core in an analogous manner, producing the respective *hetero*metal clusters. Addition of the closed-shell d metal ions Zn^{2+} or Cd^{2+} to the reduced core $[3Fe\text{-}4S]^0$ should generate a heteroatom cluster (respectively $[Zn3Fe\text{-}4S]^{2+}$ or $[Cd3Fe\text{-}4S]^{2+}$), which is formally isoelectronic in valence d electrons with $[3Fe\text{-}4S]^0$ and gives a noninteger spin system upon one-electron reduction ($[Zn3Fe\text{-}4S]^+$ and $[Cd3Fe\text{-}4S]^+$). We therefore prepared samples of Zn and Cd products for spectroscopy.

Following two-electron bulk electrolytic reduction of the 7Fe protein, additions of aliquots of Zn^{2+} or Cd^{2+} produced stepwise increases in the bulk reduction current obtained at −680 and −750 mV, respectively. By analogy with previous titrations[3] carried out for uptake of Fe^{2+} (correcting for preferential complexation of the first additions of Zn^{2+} by EGTA or of Cd^{2+} by HPDTA), complete formation of a new reducible species was achieved upon addition of the equivalent of one M^{2+} per protein molecule (actual results obtained were 1.02 Zn^{2+} and 0.94 Cd^{2+}). Care was taken not to add excess Cd^{2+} since, at the sustained low potential (ca. −700 mV) required to reduce the product substantially, deposition of Cd^0 occurred as indicated by the presence of a sharp anodic stripping wave in the cyclic voltammogram. Reduced products were collected for examination by EPR after continued electrolysis (after passage of a further 0.6–1.0 electron equivalent). For the Zn product, chemical titration as described above was used to obtain a more concentrated sample (300 μM).

The resulting EPR spectra are shown in Figure 4. In each case (not shown) the $[4Fe\text{-}4S]^+$ cluster of the original 7Fe ferredoxin (i.e., the indigenous cluster) could be observed clearly in the region at $g \sim 2$. Double integration of this signal gave approximately 0.996 spin for M = Zn and 0.702 spin for M = Cd, showing, first, that most if not all of the indigenous cluster population had been reduced and, second, that the "new" heteroatom cluster was not contributing any significant number of spins in this region of the EPR spectrum. The region of the spectrum around $g = 4$–5 contains, in both cases, a rather broad, derivative shaped signal that is not characteristic of adventitious Fe(III) ion (which gives rise to a much sharper signal). It is most unlikely, in any case, that Fe(III) would be found under such conditions of low potential. As now discussed, the signals can be assigned to the $M_s = \pm^3/_2$ middle Kramers's doublet of an $S = {}^5/_2$ state.

In the case of $[Zn3Fe\text{-}4S]^+$ the EPR signals are observed at $g = 4.46$ and 4.01 (see Figure 4a). In addition, two broad absorption shaped signals at $g = 9.6$ and ~8.8 are detected at very low temperatures. Their relative intensities vary strongly with temperature over the range 4–10 K. The signal at $g = 9.6$ is the most intense at low temperature but decreases in intensity on warming whereas the broad feature at $g \sim 8.8$ increases in intensity. However, both signals broaden and weaken above 8.0 K. Together, these results indicate that the $[Zn3Fe\text{-}4S]^+$ cluster has spin $S = {}^5/_2$ subject to a rather small zero-field splitting. The temperature variation of the two signals at $g = 9.6$ and ~8.8 shows that they can be assigned to the lowest and highest of three Kramers' doublets of the $S = {}^5/_2$ ground state. The g values do not fit well a spin Hamiltonian under the assumption that $h\nu \ll |D|$, where $h\nu$ is the microwave energy (~0.3 cm^{-1}) and D is the axial zero-field splitting parameter. This implies a smaller value for D in the $[Zn3Fe\text{-}4S]^+$ cluster of Fd III compared to the value of -2.7 ± 0.5 cm^{-1} reported for the corresponding cluster generated in Fd II from *D. gigas*.[6] The steeper temperature dependence of the signals in the region $g \approx 9$ for the Fd III cluster compared with Fd II also provides confirmation of this. In the latter case,

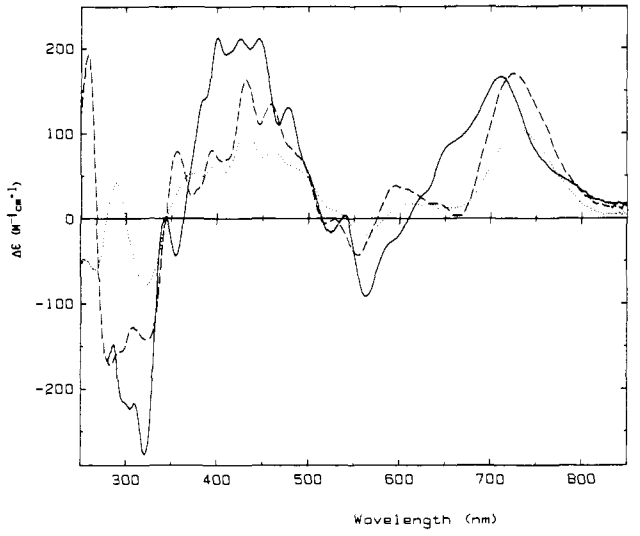

Figure 5. MCD spectra of $[3Fe\text{-}4S]^0$ (—), and $[M3Fe\text{-}4S]^{2+}$ where M = Zn (- - -) and M = Cd (···), measured at 1.6 K and 5 T (path length 1 mm). $[3Fe\text{-}4S]^0$: Fd III, 361 μM; 20 mM Hepes buffer, pH 7.4, 0.2 M NaCl and 50% (v/v) ED; sample prepared by addition of reduced phenosafranine. $[Zn3Fe\text{-}4S]^{2+}$: Fd III, 275 μM; $ZnSO_4$, 890 μM; 0.1 M Taps buffer, pH 8.2, 0.2 M KCl and 50% (v/v) ED including 20 μM of mediator dyes; sample titrated with $Na_2S_2O_4$ to −315 mV vs SHE. $[Cd3Fe\text{-}4S]^{2+}$: Fd III, 220 μM; $CdCl_2$, 715 μM; 0.4 M Hepes buffer, pH 7.6, 0.2 M KCl and 50% (v/v) ED including mediator dyes; sample titrated with $Na_2S_2O_4$ to −275 mV vs SHE.

the signals at $g = 9.8$ and 9.3 are clearly observable at 15 K. As shown in Figure 4b, a similar EPR spectrum, with g values 4.54 and 4.14, was observed for the $[Cd3Fe\text{-}4S]^+$ cluster. Here, however, the low-field signals were too weak to detect due to the lower protein concentration required for efficient bulk electrolysis.

The EPR spectra of the oxidized products were each devoid of significant features in the regions of $g = 2$ and 4.3, but the low-field region, $g \approx 12$, showed a broad negative trough similar to that detected for $[3Fe\text{-}4S]^0$ clusters.[22] The MCD spectra of Zn and Cd oxidized products, and the reduced $[3Fe\text{-}4S]^0$ cluster at 1.6 K and 5 T are compared in Figure 5. The spectra are broadly similar but reveal interesting changes in detail. The region at wavelength <400 nm shows most variation. This is the spectral region in which localized Cd(II) transitions, $d^{10} \rightarrow$ s or p are expected and where $S^{2-} \rightarrow$ Cd(II) charge-transfer bands may arise. In the visible region, MCD spectra are dominated by optical transitions associated with the $[3Fe\text{-}4S]^0$ fragment. At these wavelengths, there is no major change in the spectral features yet the fact that shifts are observed lends further support for the formation of heteroatom clusters in which Zn or Cd have become incorporated and are coordinated, most plausibly to the open corner of the [3Fe-4S] core structure through the three μ_2-S atoms. These results, however, give no indication of the likely ligand(s) to the heterometal opposite to the μ-sulfido ligation. The carboxylate side chain of aspartate, Asp-14, is one obvious candidate, as we have discussed previously[3] for the transformed [4Fe-4S] cluster. However, we cannot rule out H_2O or OH^- as ligands.

Figure 6 shows the MCD magnetization curves of the three clusters $[3Fe\text{-}4S]^0$, $[Zn3Fe\text{-}4S]^{2+}$, and $[Cd3Fe\text{-}4S]^{2+}$ measured at the peak maximum of the band between 700 and 750 nm. The curves were recorded at 1.6 K between 0 and 5 T. It is now established that, in the case of the $[3Fe\text{-}4S]^0$ cluster of Fd II, *D. gigas*, the electronic ground state is $S = 2$, which undergoes an axial zero-field splitting of negative sign[23] and value $D \simeq -2.7$ cm^{-1}.[24] This leads to a doublet $M_s = \pm 2$ as the lowest component

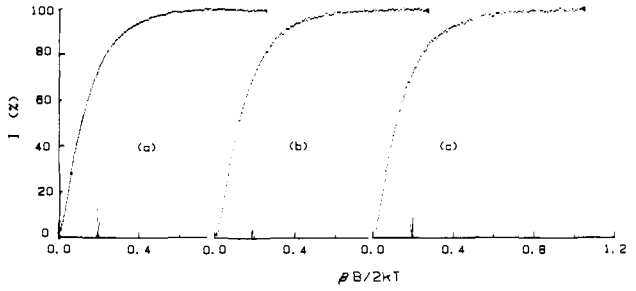

Figure 6. MCD magnetization curves: (a) $[3Fe\text{-}4S]^{2+}$ at 712 nm; (b) $[Zn3Fe\text{-}4S]^{2+}$ at 727 nm; (c) $[Cd3Fe\text{-}4S]^{2+}$ at 732 nm. Spectra recorded at 1.6 K between 0 and 5 T. Intercept (I) and $g_\parallel$ values are as follows: (a) 0.195, 7.66; (b) 0.191, 7.83; (c) 0.197, 7.60.

Scheme I

$$[3Fe\text{-}4S]^{1+} \overset{A'}{\rightleftharpoons} [3Fe\text{-}4S]^0 \overset{C'}{\rightleftharpoons} [3Fe\text{-}4S]^{2-} \quad (?)$$

labile cluster

$$(K_d) \Vert M^{2+}$$

$$[M3Fe\text{-}4S]^{2+} \overset{D'}{\rightleftharpoons} [M3Fe\text{-}4S]^{1+}$$

stable cluster

$$[4Fe\text{-}4S]^{2+} \overset{B'}{\rightleftharpoons} [4Fe\text{-}4S]^{1+}$$

of the ground state, lying ~9 cm^{-1} below the next higher level. This doublet has effective g values of $g_\parallel = 8.0$ and $g_\perp = 0.0$. The MCD magnetization curve for an x,y-polarized optical transition from this doublet is predicted to have an intercept value $I = 0.185$.[23] I is defined as the ratio of the magnetization limit to the initial Curie low slope and was introduced as a convenient index of the ground state g values.[25] The prominent positive peak between 700 and 750 nm in the MCD spectra of the $[3Fe\text{-}4S]^0$ cluster in a variety of ferredoxins displays an MCD magnetization curve at 1.5–1.6 K with I values close to 0.185 and can therefore be taken to have x,y polarization relative to the **g** tensor framework. The three magnetization curves shown in Figure 6 have I values of 0.195, 0.191, and 0.197; the corresponding $g_\parallel$ values derived from these are 7.66, 7.83, and 7.60, respectively. This comparison shows that the two oxidized heterometal clusters have a ground-state spin $S = 2$, with a negative axial zero-field splitting parameter D. This is consistent with the presence of the broad EPR signal at low field, which has been assigned to the $\Delta M_s = \pm 4$ transition within the $M_s = \pm 2$ ground doublet. Further analysis of the temperature dependence of the MCD spectra suggests that the D values are altered only slightly when either Zn(II) or Cd(II) is bound to the cluster.

On the basis of the similarity between solution and adsorbed film voltammetry, and from the weight of corresponding electrochemical and spectroscopic evidence, we assign the new couples D′ produced by transformations within the adsorbed protein films as being $[4Fe\text{-}4S]^{2+/+}$, $[Zn3Fe\text{-}4S]^{2+/+}$, and $[Cd3Fe\text{-}4S]^{2+/+}$. The voltammetric observations are summarized in Scheme I.

Our studies indicated, furthermore, that Zn^{2+} or Cd^{2+} is taken up by $[3Fe\text{-}4S]^0$ with a higher affinity than is exhibited for Fe^{2+}. This could indeed be confirmed qualitatively by competition experiments, in which a film of 7Fe Fd III was transferred to a buffer–electrolyte solution containing equal concentrations (typically 1 μM in each) of Fe^{2+} and Zn^{2+} or of Fe^{2+} and Cd^{2+}. The resulting voltammograms were dominated by the appearance of signals (couple D′) corresponding to [Zn3Fe-4S] or [Cd3Fe-4S] species. We thus proceeded to make a more quantitative assessment of the equilibria.

(22) Hagen, W. R.; Dunham, W. R.; Johnson, M. K.; Fee, J. A. *Biochim. Biophys. Acta* **1985**, *828*, 369.
(23) Thomson, A. J.; Robinson, A. E.; Johnson, M. K.; Moura, J. J. G.; Moura, I.; Xavier, A. V.; LeGall, J. *Biochim. Biophys. Acta* **1981**, *670*, 93.
(24) Day, E. P.; Peterson, J.; Bonvoisin, J. J.; Moura, I.; Moura, J. J. G. *J. Biol. Chem.* **1988**, *263*, 3684.
(25) Thomson, A. J.; Johnson, M. K. *Biochem. J.* **1980**, *191*, 411.

For the transformation equilibrium described by reaction 1, the dissociation constant K_d is defined by

$$K_d = \frac{\{[3Fe\text{-}4S]^0\}\{M^{2+}\}}{\{[M3Fe\text{-}4S]^{2+}\}} \quad (2)$$

For protein molecules confined to the electrode, $\{[3Fe\text{-}4S]^0\}$ and $\{[M3Fe\text{-}4S]^{2+}\}$ are surface populations. Since the total cluster population is negligible compared to the amount of M^{2+} in the electrolyte, the term $\{M^{2+}\}$ is equal to the initial bulk concentration of M^{2+}.[26] Thus, we can write a simple expression (3) relating the equilibrium ratio of [M3Fe-4S] to [3Fe-4S] clusters with the concentration of M^{2+} in the electrolyte.

$$\frac{\{[M3Fe\text{-}4S]^{2+}\}}{\{[3Fe\text{-}4S]^0\}} = \{M^{2+}\}\frac{1}{K_d} \quad (3)$$

We determined K_d for the reaction occurring in the film under the control of the applied potential. To do this, we transferred electrodes that had been coated with the 7Fe ferredoxin (and cycled successively in buffer electrolyte in the normal manner) into sample pots containing various concentrations of Fe^{2+}, Zn^{2+}, or Cd^{2+}. Such solutions were stirred by microflea. By applying a fixed electrode potential (the "base" potential) in the region between (and optimally separated from) $E^{0'}$ for the couples $[3Fe\text{-}4S]^{+/0}$ and $[M3Fe\text{-}4S]^{2+/+}$, we could ensure that the oxidation levels were held at those necessary to conform to the simple equilibrium defined by eq 2. Then, after adequate time had been allowed for equilibrium to be established, the population ratio $\{[M3Fe\text{-}4S]\}/\{[3Fe\text{-}4S]\}$ was sampled as shown in Figure 7 (upper) by executing a single, rapid cycle across waves A′ and D′ without traversing couple C′. To convert the observed populations into values for K_d, it was necessary to assume that rates of relaxation to new equilibrium positions (in response to the temporarily induced changes in cluster oxidation levels) were slow compared to the rate at which the potential is cycled for sampling (470 mV s^{-1}). Checks on the rates of metal ion entry (A′ → D′) and release (D′ → A′) under cycling conditions showed that this was a reasonable assumption at the low levels of M^{2+} used.

Two types of numerical procedure were used to estimate equilibrium population ratios. Primarily, for all M^{2+}, the population ratio at each concentration (after equilibrating at a potential between D′ and A′) was determined by inspection of current amplitudes observed at oxidative wave A′ for zero $\{M^{2+}\}$, saturating (high) $\{M^{2+}\}$, and intermediate $\{M^{2+}\}$ levels. The changes Δi_{equil} and Δi_{total} were determined as illustrated in Figure 7 (upper). From these values, the respective fractions f_{3Fe} ($=\Delta i_{equil}(A')/\Delta i_{total}(A')$) and then $f_{M3Fe} = 1 - f_{3Fe}$ were obtained. The quotient $(1 - f_{3Fe})/f_{3Fe}$ was then adopted as a measure of the population ratio $\{[M3Fe\text{-}4S]\}/\{[3Fe\text{-}4S]\}$. Determinations were carried out several times for each M^{2+} concentration. As depicted in Figure 7 (lower), plots of the population ratio $\{[M3Fe\text{-}4S]\}/\{[3Fe\text{-}4S]\}$ against $\{M^{2+}\}$ each gave straight lines, as expected.[27] In a secondary procedure, we estimated $\{[M3Fe\text{-}4S]\}$ directly by analogous inspection of waves D′. From this we determined f_{M3Fe} independently and recomputed the data using the quotient f_{M3Fe}/f_{3Fe}. (Note that as shown in Figure 7 (upper), the apparent contributions from $D'_{(Zn)}$ are less than those for A′. This is because of the closeness of the lower limit switching potential, necessary to avoid passage through C′, and the finite response time for sweep reversal at 470 mV s^{-1}.) Such a procedure was inappropriate for Cd^{2+} since the significant overlap of waves D′ and C′ entirely prevented independent measurement. The outcome of this test was that values of K_d obtained for Fe^{2+} and Zn^{2+} did not vary significantly between either numerical procedure, thus providing us with acceptable confidence in the approach. Results are tabulated in Table I, which includes a compilation of reduction potentials for each cluster type. Since the similarity in K_d values

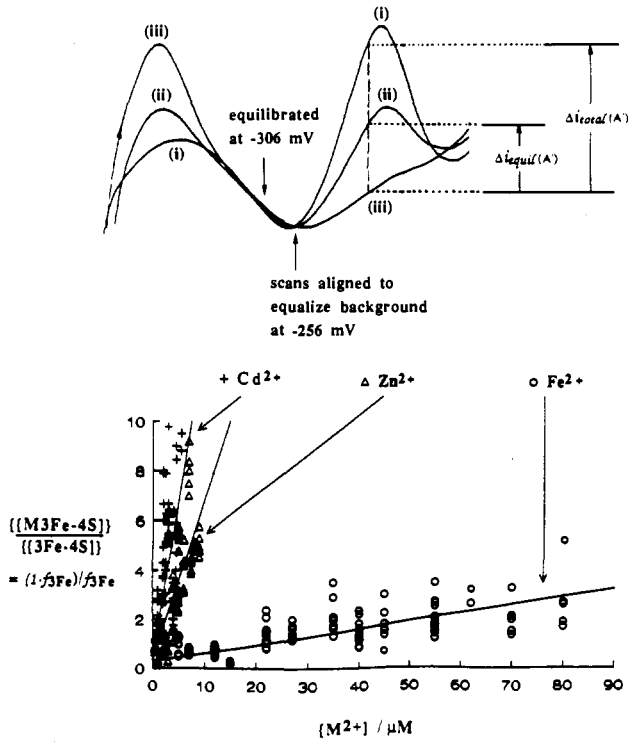

Figure 7. Upper: Example illustrating the measurement of Δi_{equil} and Δi_{total}, from which the population ratio $(1 - f_{3Fe})/f_{3Fe}$ was determined for various $\{M^{2+}\}$. Oxidative scans (470 mV s^{-1}) showing appearance of waves A′ and D′ after equilibration at 0 °C in (i) buffer electrolyte containing 10 μM EGTA, (ii) buffer electrolyte containing 1 μM Zn^{2+}, and (iii) buffer electrolyte containing 20 μM Zn^{2+}. Lower: Graph showing the dependence of cluster population ratio $\{[M3Fe\text{-}4S]\}/\{[3Fe\text{-}4S]\}$ on the concentration of M^{2+} in the buffer electrolyte (no EGTA). Lines were computed by a linear regression program. Films of ferredoxin III were prepared as described in the text and precycled in buffer electrolyte containing 10 μM EGTA, before being transferred to a stirred pot containing a known concentration of M^{2+}. Separate experiments were carried out for each data point. Equilibrium was established at 0 °C and measured as follows. Fe: potential held at −256 mV for 2 min prior to scan; population ratio $\{[4Fe\text{-}4S]\}/\{[3Fe\text{-}4S]\}$ determined from $(1 - f_{3Fe})/f_{3Fe}$ (see text). Currents were measured and compared at −131 mV ([3Fe-4S]). The value of K_d determined instead from f_{4Fe}/f_{3Fe} (independently estimating the contribution from [4Fe-4S] at −406 mV; see text) is in good agreement (see Table I). Zn: potential held at −306 (or −256 mV) for 2 min; population ratio $\{[Zn3Fe\text{-}4S]\}/\{[3Fe\text{-}4S]\}$ determined from $(1 - f_{3Fe})/f_{3Fe}$ (see text). Currents were measured and compared at −131 mV ([3Fe-4S]). The value of K_d determined instead from f_{Zn3Fe}/f_{3Fe} (independently estimating the contribution from [Zn3Fe-4S] at −481 mV; see text) is in good agreement (see Table I). Cd: potential held at −346 mV for 2 min; population ratio $\{[Cd3Fe\text{-}4S]\}/\{[3Fe\text{-}4S]\}$ determined from $(1 - f_{3Fe})/f_{3Fe}$ (see text). Currents were measured and compared at −131 mV ([3Fe-4S]).

Table I

	$K_d/\mu M$		$E^{0'}([M3Fe\text{-}4S]^{2+/+})$/ mV vs SHE	
M^{2+}	$(1 - f_{3Fe})/f_{M3Fe}$	f_{M3Fe}/f_{3Fe}	film	solution
Fe	30 ± 15	29 ± 14	−393 ± 10	−400 ± 15
Zn	1.6 ± 1.0	1.6 ± 1.0	−492 ± 10	−480 ± 15
Cd	0.8 ± 0.5		−569 ± 10	−580 ± 10

(26) In using the bulk solution concentration of M^{2+}, we have ignored local alterations in ionic activity close to the electrode due to the potential profile of the Gouy–Chapman–Stern layer. However, to test whether the order of K_d ($Cd^{2+} \leq Zn^{2+} \ll Fe^{2+}$) was influenced by the increasingly more negative applied base potentials, we varied this parameter in several determinations. For example, K_d for Zn^{2+} was determined from a base potential identical with that used for Fe^{2+}. We found no significant difference in our results. For nonspecific effects, the influence of applied electrode potential on the diffuse layer concentrations of each M^{2+} ion is expected to be the same. (See, for example: Bard, A. J.; Faulkner, L. R., *Electrochemical Methods*; Wiley: 1980; Chapter 12.)

(27) Alternatively, plots of log ($\{[M3Fe\text{-}4S]\}/\{[3Fe\text{-}4S]\}$) ($y$) against log $\{M^{2+}\}$ (x) yielded straight lines intercepting the abscissa ($y = 0$) axis at log K_d. These were in good agreement with values determined by the direct non-log graph, and gradients were each consistent with a 1/1 equilibrium as determined independently by bulk solution titration.

for M = Zn^{2+} and Cd^{2+} was within the error margins, a clearer distinction was made through a further direct competition experiment. Transfer of a film of 7Fe Fd III into buffer electrolyte solutions containing a equal concentration of Zn^{2+} and Cd^{2+} (1-5 μM in each, prepared by dilution of a concentrated 1/1 stock solution) produced, after equilibration at -300 mV, voltammograms that were dominated by D′ signals due to $[Cd3Fe\text{-}4S]^{2+/+}$. When the Zn/Cd stoichiometry was raised to 2/1, D′ signals due to $[Zn3Fe\text{-}4S]^{2+/+}$ and $[Cd3Fe\text{-}4S]^{2+/+}$ appeared at approximately equal amplitude. Thus, we may conclude that the order of K_d values is as expected[28] for a divalent metal ion coordinated to a sulfide-rich site; that is, $Cd^{2+} \geq Zn^{2+} \gg Fe^{2+}$.

For a wider evaluation, analogous experiments were carried out on the [3Fe-4S],[4Fe-4S] ferredoxin I from *Azotobacter chroococcum*. This protein also gave a stable film displaying three pairs of waves. However, the form of the voltammogram was *unchanged* following a period of at least 30-min voltammetric cycling in solutions (pH 7) containing Fe^{2+} (3 mM), Zn^{2+} (3 mM), or Cd^{2+} (15 μM). This absence of reactivity of the 3Fe cluster in this protein was confirmed by experiments undertaken on a bulk solution.

The broad implication from these studies is that the voltammetry of a protein that is confined to an electrode surface as a molecular film (and is thus readily transferable between various solutions) can be extremely informative, providing an accurate reflection of complicated chemistry that occurs in bulk solution. As a surface electrochemical technique, it presents a highly sensitive and specific analytical method for viewing and controlling the chemistry of active sites in the time domain. In the example that we have described, the formation of specific cluster species, undefined by all but sophisticated low-temperature spectroscopic methods, is clearly observed through the appearance of well-defined voltammetric signals. As a quantitative tool for the determination of equilibrium and kinetic parameters, the approach should permit the investigation of a rich and complex chemistry associated with labile clusters. The results show that, in Fd III, the $[3Fe\text{-}4S]^0$ cluster readily binds additional divalent metal ions in an equilibrium process that is rapidly established, with an affinity order $Cd^{2+} \geq Zn^{2+} \gg Fe^{2+}$. Furthermore, the binding of such metal ions to produce $[M3Fe\text{-}4S]^{2+}$ is relatively weak, and the $\{[M3Fe\text{-}4S]\}/\{[3Fe\text{-}4S]\}$ population ratio can be effectively modulated by variations in the M^{2+} identity and its activity across a range 10^{-4}-10^{-6} M. Little is known about the relative available concentrations of Fe^{2+} and Zn^{2+} within the cells of obligate anaerobic bacteria such as *D. africanus*. However, if these conclusions prove to be more general, it is important to be aware of the possibility that heterometal-sulfur clusters of the type described here may exist naturally in some proteins. Furthermore, the demonstrated capability for rapid interconversion equilibria might be exploited for some regulatory purpose. The latter possibility is indeed suggested in the recent report by Rouault et al.[29] concerning the sequence similarity between aconitase and a mRNA binding protein—the "iron-responsive element binding protein" (IRE-BP)—that links the expression of ferritin and of the transferrin receptor to Fe levels in the cell.

Acknowledgment. This work was supported by the University of California and grants from NATO (CRG 900302), from the Molecular Recognition Initiative of the SERC of the U.K., and by an Exxon Education Foundation Award (F.A.A.). We are grateful to Dr. A. Sucheta for assistance with data analysis.

Registry No. Fe^{2+}, 7439-89-6; Zn^{2+}, 7440-66-6; Cd^{2+}, 7440-43-9.

(28) See, for example: Phillips, C. S. G.; Williams, R. J. P. *Inorganic Chemistry*; Oxford University Press: Oxford, 1965; Vol. I, p 630.

(29) Rouault, T. A.; Stout, C. D.; Kaptain, S.; Harford, J. B.; Klausner, R. D. *Cell* **1991**, *64*, 881.

Communications to the Editor

Antibody-Catalyzed Bimolecular Imine Formation

Andrea G. Cochran,† Tony Pham,† Renee Sugasawara,‡ and Peter G. Schultz*,†

Department of Chemistry, University of California Berkeley, California 94720
Igen, Inc., 1530 East Jefferson Street Rockville. Maryland 20852
Received May 9, 1991

Recently chemists have enlisted the cellular machinery of the immune system to produce highly selective catalysts.[1-3] One of several strategies for generating catalytic antibodies is the use of antibody affinity and specificity to bind both substrate and a cofactor in a catalytically productive orientation. Pyridoxal phosphate (PLP) is a versatile enzymatic cofactor which is commonly involved in reactions of α-amino acids involving carbanion intermediates.[4] The reactions catalyzed by this cofactor include transamination, decarboxylation, racemization, and β- and γ-elimination. Transamination, in particular, is a well-studied reaction, both by enzymologists[5-8] and by organic chemists.[9-11] The mechanistic interest in this reaction as well as the importance of chiral α-amino acids in biological studies and as synthetic intermediates suggest transamination as a target for antibody catalysis.

One of the earliest attempts to generate catalytic antibodies was reported by Raso and Stollar, who, in 1975, generated antibodies to a reduced aldimine formed from 3-aminotyrosine and PLP.[12-14] Although these polyclonal antibodies did not display any significant catalytic properties, it was demonstrated that amino acid, PLP, and aldimine were bound by the antibody. We prepared hapten (**1**) via reductive amination of pyridoxal with L-*p*-nitrophenylalanine and sodium borohydride. The 5′-hydroxyl group of the cofactor was then converted to a thiol via the isothiuronium salt, activated with 2,2′-dithiodipyridine, and

* To whom correspondence should be addressed.
† University of California.
‡ Igen, Inc.

(1) Schultz, P. G. *Angew. Chem. Int. Ed. Engl.* **1989**, *28*, 1283-1295.
(2) Shokat, K. M.; Schultz, P. G. *Ann. Rev. Immunol.* **1990**, *8*, 335-63.
(3) Lerner, R. A.; Benkovic, S. J.; Schultz, P. G. *Science* **1991**, *252*, 659.
(4) Walsh, C. *Enzymatic Reaction Mechanisms*; W. H. Freeman: New York, 1979; Chapter 24.
(5) Toney, M. D.; Kirsch, J. F. *Science (Washington, D.C.)* **1989**, *243*, 1485-1488.
(6) Julin, D. A.; Wiesinger, H.; Toney, M. D.; Kirsch, J. F. *Biochemistry* **1989**, *28*, 3815-3821.
(7) Julin, D. A.; Kirsch, J. F. *Biochemistry* **1989**, *28*, 3825-3833.
(8) McLeish, M. J.; Julin, D. A.; Kirsch, J. F. *Biochemistry* **1989**, *28*, 3821-3825.
(9) Bruice, T. C.; Benkovic, S. *Bioorganic Mechanisms*; W. A. Benjamin: New York, 1966; Chapter 8.
(10) Leussing, D. L. In *Vitamin B_6. Pyridoxal Phosphate*; Dolphin, D., Poulson, R., Avramovic, O., Eds.; Wiley: New York, 1986; pp 69-115.
(11) Breslow, R.; Czarnik, A. W.; Lauer, M.; Leppkes, R.; Winkler, J.; Zimmerman, S. *J. Am. Chem. Soc.* **1986**, *108*, 1969-1979.
(12) Raso, V.; Stollar, B. D. *J. Am. Chem. Soc.* **1973**, *95*, 1621-1628.
(13) Raso, V.; Stollar, B. D. *Biochemistry* **1975**, *14*, 584-591.
(14) Raso, V.; Stollar, B. D. *Biochemistry* **1975**, *14*, 591-599.

0002-7863/91/1513-6670$02.50/0